Cell Reports
Physical Science

CellPress
OPEN ACCESS

Article

A cost-effective water-in-salt electrolyte enables highly stable operation of a 2.15-V aqueous lithium-ion battery

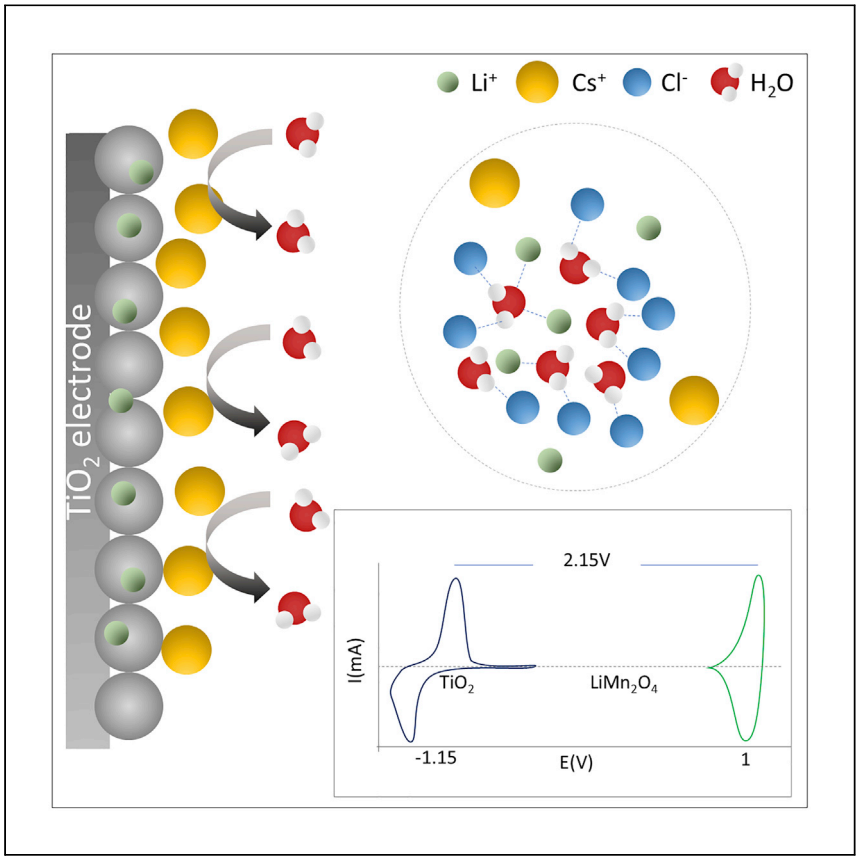

The need for safe and cost-effective energy storage systems has advanced the development of aqueous batteries. Looking for a cost-effective electrolyte solution, Turgeman et al. propose saturated LiCl + 4 M CsCl. It is found that addition of CsCl significantly improves electrolyte stability and enables stable operation of a 2.15-V battery.

Meital Turgeman, Vered Wineman-Fisher, Fyodor Malchik, ..., Dan Thomas Major, Netanel Shpigel, Doron Aurbach

nshpigel@gmail.com

Highlights

Mixed aqueous LiCl + CsCl electrolyte solution enables widely stable electrochemical window

Cl^- anions interact with the free H_2O molecules and reduce their bulk activity

The added chaotropic Cs^+ cations adsorb on the anode interface and prevent H_2 generation

Long-term stable 2.15-V cell comprising TiO_2 anode and $LiMn_2O_4$ cathode demonstrated

Turgeman et al., Cell Reports Physical Science 3, 100688
January 19, 2022
https://doi.org/10.1016/j.xcrp.2021.100688

Cell Reports
Physical Science

CellPress
OPEN ACCESS

Article

A cost-effective water-in-salt electrolyte enables highly stable operation of a 2.15-V aqueous lithium-ion battery

Meital Turgeman,[1] Vered Wineman-Fisher,[1] Fyodor Malchik,[2] Arka Saha,[1] Gil Bergman,[1] Bar Gavriel,[1] Tirupathi Rao Penki,[1] Amey Nimkar,[1] Valeriia Baranauskaite,[3] Hagit Aviv,[1] Mikhael D. Levi,[1] Malachi Noked,[1] Dan Thomas Major,[1] Netanel Shpigel,[1,4,*] and Doron Aurbach[1]

SUMMARY

Extensive efforts are currently underway to develop safe and cost-effective electrolytes for large-scale energy storage. In this regard, water-based electrolytes may be an attractive option, but their narrow electrochemical stability window hinders their realization. Although highly concentrated fluorinated electrolytes have been shown to be highly effective in suppression of water splitting, enabling significant widening of the applied potential range, they utilize expensive salts (e.g., lithium bis(trifluoromethane sulfonyl) imide [LiTFSI] or lithium trifluoromethane sulfonate [LiOTf]); hence, they cannot be considered for practical applications. Here, we demonstrate a cost-effective aqueous electrolyte solution combining 14 M LiCl and 4 M CsCl that allows stable operation of a 2.15-V battery comprising a TiO_2 anode and $LiMn_2O_4$ cathode. Addition of CsCl to the electrolyte plays a double role in system stabilization: the added chloride anions interact with the free water molecules, whereas the chaotropic cesium cations adsorb at the electrified interface, preventing hydrogen formation.

INTRODUCTION

The alarming global warming trends and their negative consequences on the world economy and population health require a drastic reduction in CO_2 emissions. Being one of the major sources of greenhouses gas pollution, fossil fuel-based electricity generation technologies have to be replaced with environmentally friendly energy sources like sun or wind. Despite the significant improvement in the electricity production efficiency of these systems during the last decade, their intermittent nature, resulting in a fluctuating power supply, poses numerous challenges related to their integration into the existing grids designed to comply with less or non-variable energy sources. In the search for viable and cost-effective solutions for large-scale energy storage, effective rechargeable batteries are a natural solution: batteries may be relatively cheap, and they can be applied anywhere and can be easily designed and adjusted to customers' needs. Because of their high capacity, energy density, and cycle life, lithium (Li)-ion battery systems have become the leading battery technology. However, conventional Li-ion batteries are based on highly flammable organic solvents such as dimethyl carbonate and diethyl carbonate. Considering the massive electrolyte solution quantities required for large-scale energy storage by non-aqueous rechargeable batteries, these conventional electrolyte solutions pose severe safety concerns. In this context, water-based electrolyte solutions in batteries may provide optimal options in terms of safety and cost. For many years,

[1]Department of Chemistry and BINA – BIU Center for Nanotechnology and Advanced Materials, Bar-Ilan University, Ramat-Gan 5290002, Israel

[2]Center for Physical and Chemical Methods of Research and Analysis, al-Farabi Kazakh National University, 050040 Almaty, Kazakhstan

[3]Department of Chemistry, Natural Science Faculty, Ben Gurion University of Negev, Beer Sheva 84105, Israel

[4]Lead contact

*Correspondence: nshpigel@gmail.com

https://doi.org/10.1016/j.xcrp.2021.100688

aqueous electrolytes were considered impractical for rocking chair-type rechargeable batteries because of the limited potential window of water, which ranges between 1.23 V (the thermodynamic stability limit) and 1.5 V in dilute electrolyte solutions.[1] For a decade and a half after commercialization of Li-ion batteries (LIBs) in 1990, research activity regarding development of aqueous batteries remained marginal compared with aprotic Li-ion systems. A substantial breakthrough toward practical aqueous LIBs was achieved recently by Suo et al.,[2] who demonstrated significant expansion of the electrochemical stability window (ESW) of aqueous systems to 3.0 V by using a highly concentrated Li bis(trifluoromethane sulfonyl) imide (LiTFSI) electrolyte. The improved ESW was attributed to the reduced electrochemical activity of water in such a concentrated electrolyte and formation of an effective passivation layer on the negative electrode by $TFSI^-$ reduction, which suppresses hydrogen evolution.[3] The increased Li^+ concentration and electrochemical activity resulted in modulation of the cathodic intercalation potential toward more positive potential values beyond the hydrogen evolution voltage range.[4] This work paved the way for development of other aqueous systems with various saturated or nearly saturated electrolytes, enabling stable operation of LIBs and other mono- and multivalent ion batteries.[5,6] To date, LiTFSI remains the state-of-the-art electrolyte solution for aquoeous lithium batteries (ALBs), providing the highest potential window among several available water-soluble Li salts. A highly concentrated (21 M) LiTFSI electrolyte enabled 1.8-V cells based on a Mo_6S_8 (Chervel phase) anode and $LiMn_2O_4$ (LMO) cathode.

Higher voltage—2.1-V average potential—was obtained by mixing LiTFSI with 7 M Li trifluoromethane sulfonate (LiOTf). This electrolyte, termed "water in bi-salt," provided an additional widening of the ESW into more negative potentials, enabling stable operation of a full cell with a TiO_2 anode and LMO cathode. Although most of the relevant LIB cathodes operate within the ESW (0–1.3 V in the Ag/AgCl scale) far below the O_2 formation potential, only a few anodes can work stably in aqueous electrolyte solutions because of H_2 evolution, which occurs prior to the redox potential of most typical LIB anodes. Therefore, increasing the cell voltage requires development of low-voltage anodes. In search of realistic options, the working potential of TiO_2 (+1.78 V versus Li, corresponding to −1.54 V in the Ag/AgCl scale) appears to be located at the maximal negative vertex of the ESW. Notably, development of aqueous $Li_4Ti_5O_{12}$ anodes, defined by a more negative operation potential of +1.5 V (versus Li) was enabled by using a combined organic and aqueous electrolyte system, comprising LiTFSI salt in mixed dimethyl carbonate (DMC):H_2O solution.[7] Despite the significant progress obtained by using highly concentrated LiTFSI, its practical application for ALBs is doubtful, mostly because of its extremely high production costs. Using such an expensive salt cannot be considered a realistic option, particularly for large-scale energy storage where huge amounts of materials are required.

Here we present a practical implementation of a cost-effective mixed electrolyte solution containing 14 M LiCl and 4 M CsCl. Apart from the significantly lower cost, this solution enables assembly of a 2.15-V cell comprising a TiO_2 anode and LMO cathode, which showed better performance in terms of energy density, efficiency, and cyclability compared with a similar system based on concentrated LiTFSI. This improved performance is attributed to reduced hydrogen activity because the presence of Cl^- ions and formation of an electrical double layer containing hydrophobic Cs^+ ions on the anode surface. The stability of the anodes was improved further by careful optimization of the cell ingredients, including current collector selection, particle size, and electrode wettability. The proposed electrolyte systems open new directions toward formulation of new and cost-effective

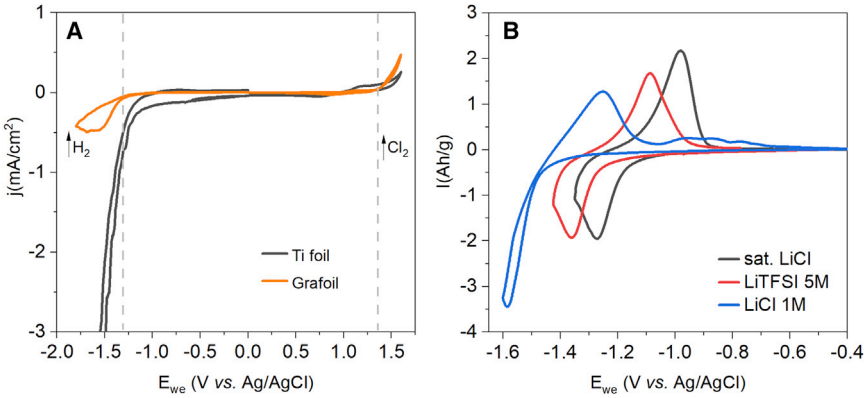

Figure 1. The dependence of the ESW on current collector type and electrolyte solution composition

(A) CVs of TiO_2 anodes coated on grafoil collected at a scan rate of 10 mV/s.

(B) ESW of neat titanium and grafoil current collectors tested by CV at 0.5 mV/s in saturated LiCl solution.

aqueous electrolyte solutions for safe and sustainable secondary batteries for large-scale energy storage.

RESULTS AND DISCUSSION

The influence of current collector and electrolyte composition on the potential stability window

The relatively low operating voltage of the TiO_2 anode (about 1.55 V versus Li or −1.69 V versus Ag/AgCl in electrolytes containing 1 M Li) entails not only utilization of a suitable electrolyte solution possessing high water splitting overpotential but also careful selection of an appropriate current collector with low catalytic activity toward the hydrogen evolution reaction (HER). Typically, for aqueous battery applications, titanium,[8] stainless steel,[9] or aluminum[10] foils are adopted as current collectors because of their good corrosion resistivity and non-catalytic character. However, the highly corrosive nature of the concentrated chloride solution limits the available options, and among the metal current collectors, only Ti can be used without severe corrosion. However, as can be seen in Figure 1A, the cathodic stability of Ti in concentrated LiCl electrolyte solution is restricted to −1.0 V, where, below this potential, a sharp decrease in the reduction current attributed to H_2 formation was observed. For this reason, it cannot be applied as a current collector for TiO_2, which has a more negative potential window. In search of an electrochemically stable current collector, the use of graphite foil (grafoil) was evaluated as an electrochemically stable current collector in a saturated LiCl solution. As shown in Figure 1A, an extended negative range up to −1.3 V versus Ag/AgCl was obtained for neat grafoil film. Encouraged by this stability, the electrochemical performance of TiO_2-coated grafoil films was evaluated in a concentrated LiCl electrolyte solution. Its advantage over the dilute (1 M) LiCl and 5 M LiTFSI electrolytes can be seen in Figure 1B. The high Li concentration in the 14 M LiCl solution results in a significant positive shift of the redox potential by more than 300 mV compared with the 1 M solution and by about 100 mV compared with 5 M LiTFSI. The high water activity in the dilute LiCl solution led to pronounced hydrogen formation, expressed by a steep decrease in the current at the negative vertex. Interestingly, at this low concentration, one can observe a second oxidation peak spread over a large potential range (−1.1 to –0.4 V), which can be ascribed to de-insertion of protons generated in the low-voltage regimen.[11]

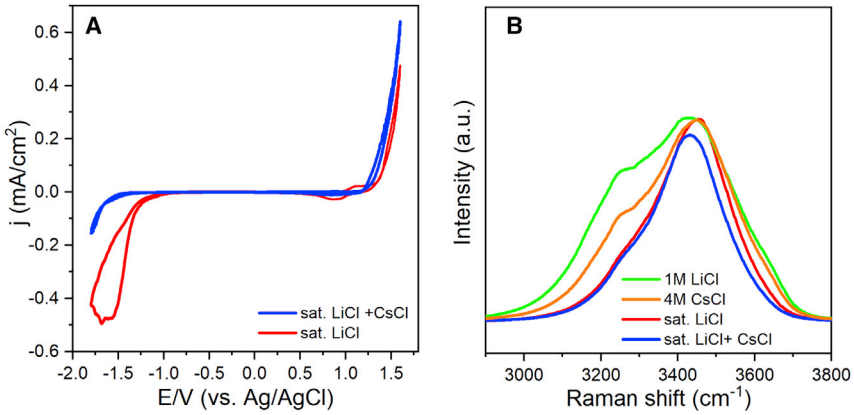

Figure 2. The effect of Cs addition as reflected by CV measurements and Raman spectra

(A) ESW window tested by CV measurements at 0.5 mV/s for saturated LiCl and mixed Li-Cs electrolytes.

(B) Raman spectra collected for various Cs and Li chloride concentrations.

The role of CsCl in system stabilization

Raman OH stretch band spectra collected for 1 M LiCl, 4.5 M CsCl, 14 M LiCl, and mixed Li-Cs chloride (14 M + 4 M) electrolytes are shown in Figure 2B. Typically, OH Raman spectra of water or dilute aqueous solutions can be deconvoluted into five main peaks (Figure S1), where the low-frequency peaks (at approximately 3,074 and 3,233 cm^{-1}) are related to symmetric OH vibrations of tetrahedrally arranged water (i.e., double donor-double acceptor configuration). The bands at 3,430 and 3,565 cm^{-1} are assigned to symmetric OH vibrations arranged in single and double donor-single acceptor configurations, respectively. The last peak, positioned at 3,633 cm^{-1}, is attributed to the OH stretching mode of bulk-like water molcules.[12,13] As can be seen in Figure 2B, a wide OH spectrum containing all of the vibrational modes was obtained for the 1 M LiCl solution. A pronounced decrease in the symmetric OH vibration peak, expressed by spectral narrowing toward high frequencies, was observed for the 4 M CsCl solution because of the increased salt concentration, which results in rearrangement of the water and formation of asymmetric H···Cl bonds. Further red-shifting was recognized in saturated LiCl and mixed LiCl-CsCl solutions; for the latter solution, additional narrowing of the high-frequency regimen related to the bulk-like water vibrational mode was observed. As described earlier, this behavior is ascribed to the increased Cl^- concentration, which results in disruption of the hydrogen bonding network by replacing O-H···O with O-H···Cl^- and formation of ionic clusters.[14–16] The dissolution of CsCl into the saturated LiCl solution increases the amount of hydrogen chloride bonds in the solution and further reduces the activity of the water and, hence, the hydrogen evolution.

The obtained Raman spectra suggest that the major factor contributing to the increased HER overpotential is the addition of Cl^- ions, which interact with the available hydrogen in the electrolyte. Nevertheless, it seems that further suppression of water splitting is provided by the presence of Cs^+ in the electrolyte. Adsorption of cesium cations upon negative polarization results in formation of a Cs^+-containing electrical double layer on the electrode/electrolyte interface, which blocks water access to the electrode surface. As found by Huang et al.,[17] adsorption of chaotropic ions (i.e., water structure breakers), and particularly Cs^+ ions, which are considered highly chaotropic cations, on the electrified interface results in expulsion of interfacial water molecules and reduction of the hydrogen bonding network on the electrode surface. As is well established, formation of H_2 occurs via multiple reaction

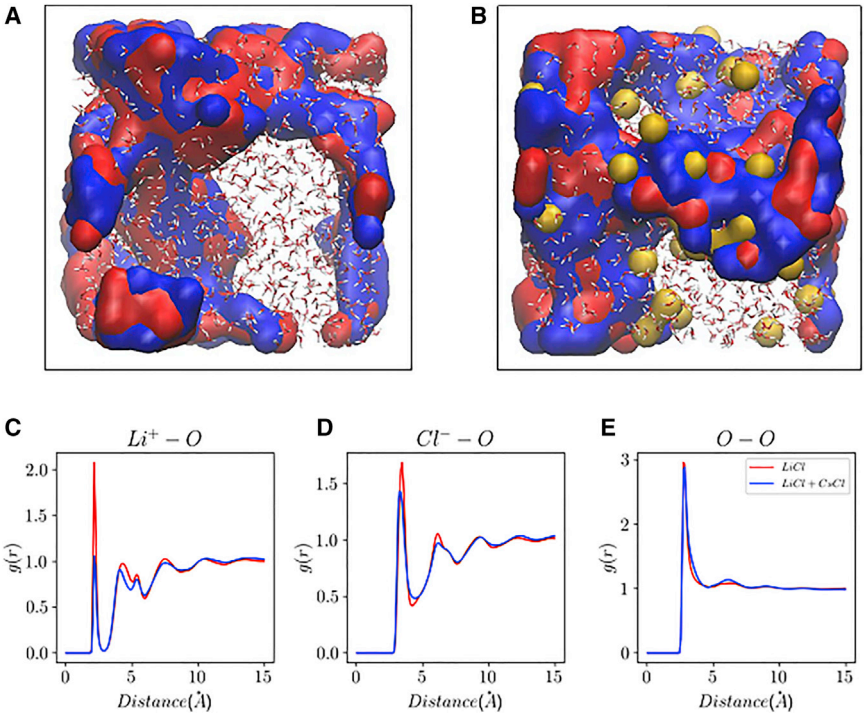

Figure 3. MD simulations of saturated LiCl and mixed LiCl + CsCl solutions

(A and B) Representative systems configurations from MD simulations of (A) 14 M LiCl and (B) 14 M LiCl + 4 M CsCl. The Li^+, Cl^-, and Cs^+ ions are colored in red, blue, and yellow, respectively. Separation to regions with bulk water and regions with a high density of ions are observed for both systems, where Cs^+ ions are also present in the bulk water regions.

(B–E) Average RDFs, g(r), of the water oxygens around Li^+ and Cl^- ions (C and D, respectively) and around water oxygens (E).

RDFs for 14 M LiCl systems are plotted in red, and RDFs for 14 M LiCl + 4 M CsCl systems are plotted in blue.

steps involving electrochemical hydrogen adsorption on the electrode surface (Volmer step), followed by interaction of the adsorbed hydrogen with solvated proton (Heyrovský reaction). The presence of Cs^+ ions on the surface and the lack of available protons on the electrode surface increase the energy barrier for the Volmer and Heyrovský steps, increasing the overpotential for H_2 formation. A similar tendency was found by Dubois et al.,[18] who demonstrated suppressed HER activity by addition of chaotropic tetrabutylammonium ions into an aqueous LiCl electrolyte.

Further understanding of the effect of CsCl on the solution structure and the ESW of the electrolyte was obtained in the present work by classical molecular dynamics (MD) simulations of 14 M LiCl and 14 M LiCl + 4 M CsCl electrolytes (for more details regarding the MD simulations and force field parameterization, see the supplemental information). The MD simulations we performed reveal regions with bulk-like water as well as regions with ionic networks in saturated LiCl and saturated LiCl + 4 M CsCl (see Figures 3A and 3B, respectively). Adding 4 M CsCl reduces the number of bulk-like water molecules. This effect is shown in Figures 3A and 3B; the LiCl electrolyte system has a greater number of bulk-like water molecules, in good agreement with the presented Raman spectra. The bulk-like water molecules tend to be arranged in partial tetrahedral networks, forming nanometric water channels that are kinetically favorable for Li-ion transport.[19] Therefore, because movement of water through these channels is preferable, the amount of water in

the vicinity of the electrode surface is expected to increase with the channel dimensions. In contrast, much narrower water channels were observed in simulations when CsCl ions were added to the solution. As can be seen in Figure 3B, the existing water channels also contain Cs^+ ions, which may diffuse through to the electrode surface and suppress H adsorption, as discussed earlier.

The average radial distribution functions (RDFs), g(r), of the water oxygens around Li^+ ions, around Cl^- ions, and around water oxygens for 14 M LiCl (red) and 14 M LiCl + 4 M CsCl (blue) are presented in Figures 3C–3E, respectively. Inspection of the RDFs reveals that there are less ordered solvation shells with less distinct peaks in the solutions with CsCl, which can be ascribed to the chaotropic nature of Cs^+ ions. The number of water molecules in the first solvation shell of Li^+ ions was reduced from 2.4 to 1.3 with addition of CsCl to the electrolyte solution. The average coordination number of water around Li^+ in the electrolyte solution with CsCl is only a third of the observed coordination number in diluted LiCl solutions, in which one Li^+ is coordinated with ~4 H_2O molecules.[20] This implies that the Li^+ ions are surrounded by several ions, mostly Cl^-, in their first shell because of the high density of ions. The number of water molecules is also reduced slightly around Cl^- ions from 4.6 to 4.4, whereas the coordination number of water around water does not change significantly. Considering a molar ratio of 2.01 water per Cl^- in the LiCl-CsCl electrolyte solutions versus 2.78 water per Cl^- in the LiCl solution, one should expect a pronounced reduction in Cl^--O interactions after CsCl addition, similar to Li-O. Nevertheless, much smaller differences were found in the Cl^--O RDF, which may imply that addition of Cl^- ions attracts water molecules from the Li^+ ion solvation shells toward the Cl^- anions.

Electrochemical performance of the TiO_2 anode in mixed LiCl + CsCl electrolyte solution

Following these conclusions, the electrochemical performance of the TiO_2 anode was evaluated for the saturated LiCl and mixed Li-Cs electrolyte solutions in half-cell configuration using an over-capacitive activated carbon cloth and Ag/AgCl as the counter and reference electrode, respectively. As presented in Figure 4, similar capacity values of 80 and 68 mAh/g were observed at high charging rates of 3 and 5 C (1 C corresponds to 335 mAh/g, the theoretical capacity of TiO_2). A still better faradaic efficiency of 99.4% and 98.8% was obtained in the mixed solution compared with 97.9% and 98.4%, which was measured in the neat LiCl electrolyte, as shown in Figures 4A and 4C, respectively. The influence of the mixed solution is relatively small because the extent of parasitic reactions is expected to decrease at higher charging rates because of kinetic limitations on H_2 formation. More significant differences were found at lower charging rates; greater charging capacities of 109.7 and 91.6 mAh/g with efficiencies of 97.3% and 99.4% were measured for 1 and 2 C, respectively (Figures 4A and 4B). As can be seen in Figures 4C and 4D, lower capacity and efficiency values of 99.4 mAh/g (94.2%) and 84.4 mAh/g (96.7%) were obtained in neat concentrated LiCl solution. Even these relatively low efficiencies obtained for LiCl salt (and *a fortiori* the high values of the mixed solution) are still higher than those obtained for the TiO_2 anode in TFSI[21,22] of acetate-based[23] electrolytes. Moreover, the relatively high conductivity of the LiCl and Li-Cs solution of 31 mS/cm allows application of relatively high charging rates while maintaining high capacity. This conductivity is significantly higher compared with previous water-in-bi-salt electrolytes comprising 21 M LiTFSI + 7 M lithium trifluoromethane sulfonate (LiOTf) or 32 M potassium acetate (KOAc) -8 M lithium acetate (LiOAc), which showed 6.5 and 5.3 mS/cm, respectively.

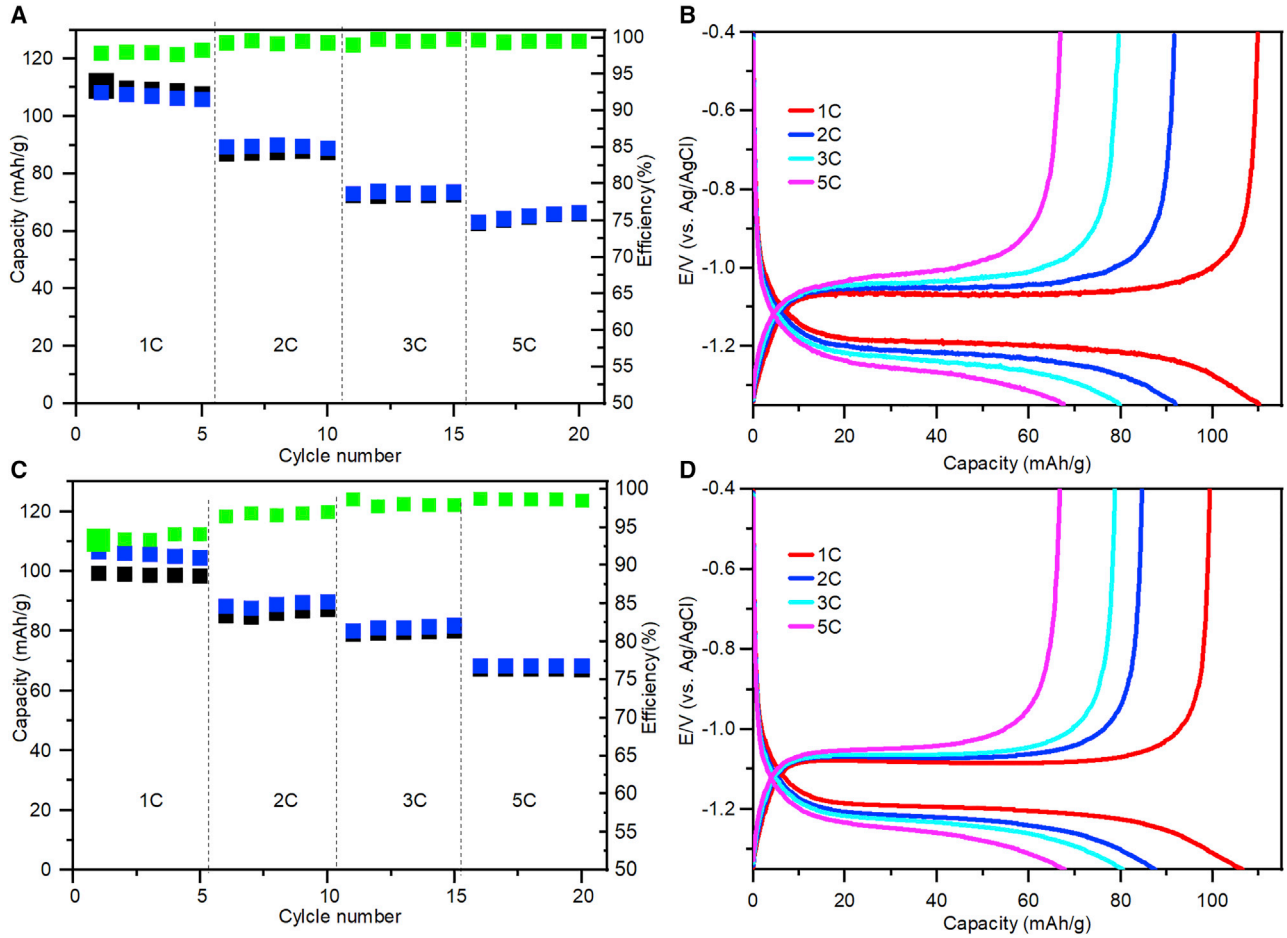

Figure 4. Electrochemical performance of saturated LiCl and mixed LiCl + CsCl solutions

(A–D) Capacity and corresponding efficiency values and GCD profiles obtained for the TiO_2 anode at different C rates for the (A and B) mixed Li-Cs and (C and D) neat LiCl electrolyte solutions.

After finding an optimized electrolyte solution, the influence of particle size on anode performance was evaluated further. For this purpose, nanometric (50-nm average size) and micrometric (3-μm average size) TiO_2 particles were chosen, as shown in Figures 5A and 5B, respectively. As indicated by XRD analyses, presented in Figure S2, both TiO_2 particles show typical spectra related to pure tetragonal anatase phase (JCPDS card number: 00-004-0477). In general, use of nanosized particles is advantageous for fast kinetics because of their short diffusion length and faster electronic transport. Nanometric particles are also beneficial for high-strain electrodes such as Si or Ga. However, the large surface area obtained by using nanoscaled particles facilitates parasitic reactions and accelerates undesirable catalytic reactions, such as oxygen or hydrogen formation. In addition, the low tap density associated with the nanoparticles resulted in a low volumetric energy density, which may be more important than the gravimetric energy density in many practical applications.[24,25]

A comparison of the cyclic voltammograms (CVs) and galvanostatic charge-discharge (GCD) profiles of the nano- and micro-sized TiO_2 anodes is presented in Figure 6. Similar Li^+ insertion/extraction voltages, defined by minimum/maximum peak current intensity at −1.3 and −0.9 V, respectively (versus Ag/AgCl), were observed at 10 mV/s for both anodes. However, although a stable response during

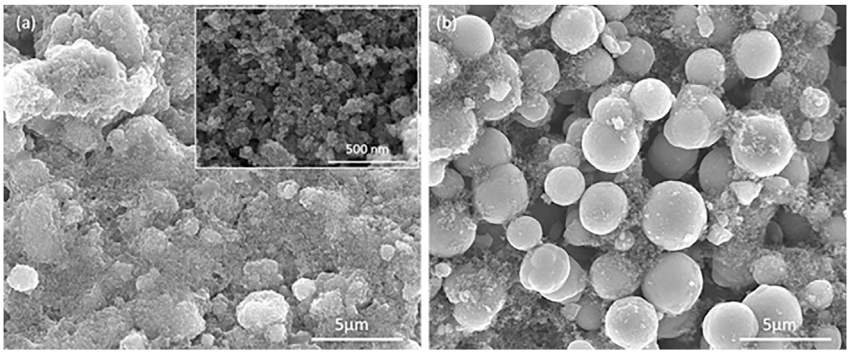

Figure 5. SEM images of nano and micro-sized TiO_2 particles

(A and B) SEM images of (A) nano-sized (inset shows an enlarged view of the nanoparticles) and (B) micro-sized TiO_2-based electrodes.

the initial cycles was obtained for the micron-sized TiO_2 anode, rapid degradation was detected for the nano-sized TiO_2. This trend is well reflected by the GCD measurements conducted at a 1 C rate (based on the theoretical capacity of TiO_2 of 335 mAh/g) for both electrodes, as shown in Figures 6C and 6D, respectively. A high-capacity value of 110 mAh/g and high Coulombic efficiency of more than 97% without any capacity fading were obtained during the initial 10 cycles with the anode with the microparticles. In contrast, a lower capacity of 90 mAh/g followed by a quick capacity loss with lower efficiency (94%) was obtained with the anode with the nanoparticles. This system presented significantly higher voltage hysteresis than the micrometric anode. Considering the low operation voltage of TiO_2, these dramatic differences can be attributed to the higher surface area of the nanoparticles, which induces nucleation and growth of nanometer-scale hydrogen bubbles that remain pinned to the surface of the nanoparticles. Therefore, the connection between the adjacent nano-sized particles provides a thermodynamically favorable interface for initial bubble nucleation. Such bubble formation blocks ion conduction pathways and leads to increased electrode resistance and voltage hysteresis.[26] Further optimization of the anode performance was obtained by improving the wettability of the electrode surface by application of Ar/O_2 plasma treatment. As can be seen in Figure S3A, poor surface wettability, expressed by the high contact angle of the Li-Cs solution on the TiO_2 surface, was obtained before the plasma treatment, whereas an excellent wettability was maintained for the plasma-treated sample (Figure S3B). The effect of the improved surface wettability on the anode performance is presented in Figures S3A and S3B, which show the CV responses of plasma-treated and untreated TiO_2 electrodes, respectively. A maximal capacity value was obtained within several cycles for the treated films, whereas a gradual capacity increase was recorded for the untreated anodes, which presented lower capacity values even after 100 cycles. Such behavior is attributed to the poor surface wettability, which prevents effective electrolyte impregnation into the electrode bulk because of the hydrophobicity of the particles.[27] Because the effect of the trapped nanobubbles and the electrode wettability on the performance is not well described in the literature, especially for aqueous systems, these findings provide useful information for further studies in which aqueous electrodes are developed.

Electrochemical characterization of full cells comprising an LMO cathode and TiO_2 anode

Encouraged by the improved performance of the optimized TiO_2 anode in the mixed Li-Cl solution, we looked for a suitable cathode that can work stably in the potential window. There are three practical options for positive electrodes that can be

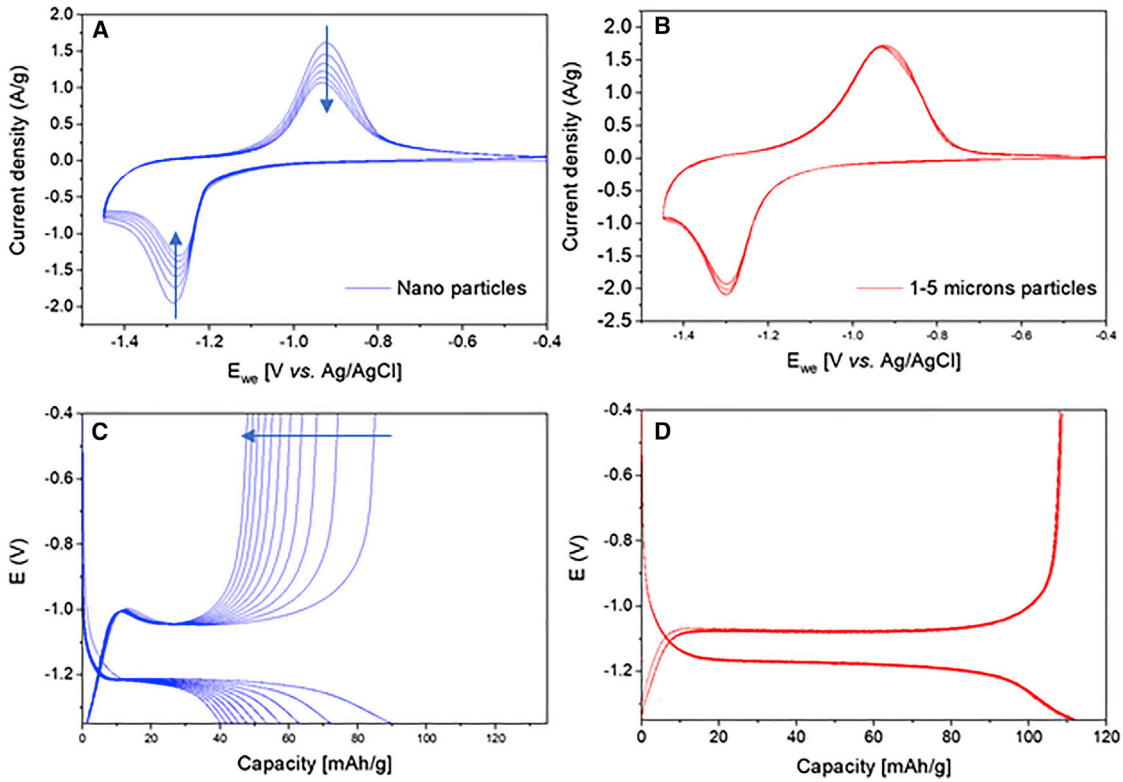

Figure 6. The influence of particles size on electrochemical performance of the anode

(A–D) CVs of (A) nano-TiO_2 and (B) micro-TiO_2 electrodes collected in mixed Li-Cs electrolyte at 10 mV/s over initial cycles and (C and D) respective GCD profiles recorded at a 1 C rate during 10 cycles.

coupled with the TiO_2 anode: V_2O_5, $LiFePO_4$ (LFP), and LMO. CVs of the three cathodes (measured at 1 mV/s) are shown in Figure 7. For clarification, the CV response of TiO_2 and the expected full cell voltages are presented as well. The maximal potential window of 2.2 V was maintained for the LMO|TiO_2 system. Because of Cl_2 formation, only the first redox couple of LMO can be obtained. Application of potentials higher than 1.25 V results in a mixed response involving Li extraction and Cl_2 evolution, as indicated by the dashed orange line in Figure 7. Nevertheless, a stable response can be obtained by limiting the potential range below 1.25 V, as demonstrated in the following section.

Focusing on the highest voltage system among the options presented above, the performance of the full cell, comprising a TiO_2 anode and LMO cathode, was evaluated. The GCD of the full cell is shown in Figure 8. A high capacity value of 97 mAh/g (based on the anode mass) and an average cell potential of 2.15 V were obtained at a 0.5 C rate. Higher charging rates of 1–5 C resulted in lower capacity values and higher voltage hysteresis, whereas at 5 C, a capacity of 57 mA/g was maintained. However, as shown in Figure 8B, high-efficiency values ranging between 96.8% in 0.5 C to 99.3% in 5 C were measured, indicating only minor to negligible contribution of the gas evolution reactions (from the negative and positive potential vertex) on the capacity. Furthermore, an impressive long-term cyclability was maintained over 1,500 GCD cycles conducted at a 5 C rate (Figure 8C). More than 87% of the initial capacity was still preserved at the last cycle. To the best of our knowledge, such a high cycling number has never been reported for an aqueous TiO_2|LMO system.

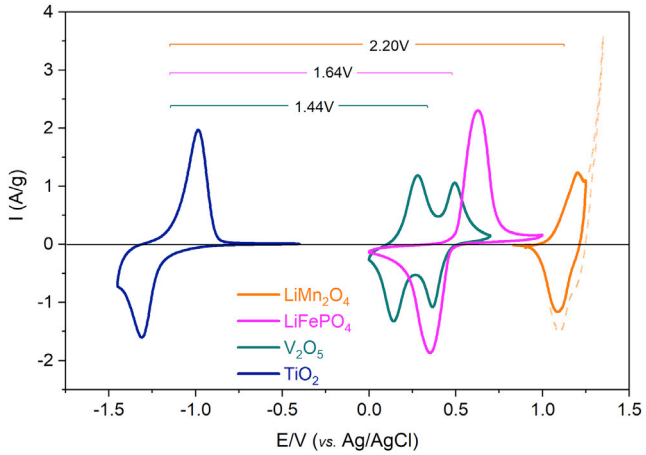

Figure 7. CVs of potential cathodes compatible with the voltage range of the mixed electrolyte
Shown are CVs recorded at a scan rate of 1 mV/s for the TiO_2 anode (green) and various cathodes: $LiMn_2O_4$ (LMO; orange), $LiFePO_4$ (LFP; pink), and V_2O_5 (black). The dashed orange line represents potential Cl_2 evolution with LMO.

Because these measurements were conducted in the T cell configuration, which is suitable for lab-level applications, a pouch cell comprising LMO|TiO_2 in LiCl-CsCl electrolyte was assembled. As shown in Figure S4A, similar capacity values were observed from the GCD profiles collected at various C rates. The long-term stability performance of the pouch cells recorded at 1 C is presented in Figure S4B. After 500 cycles, a high capacity value of 80 mAh/g was still maintained.

The self-discharge performance of the assembled pouch cells is presented in Figure S5. After 12 h at open-circuit voltage, a capacity retention of 66% was obtained. Although this behavior is far from being satisfactory for practical applications, further optimization of the system, including electrolyte systems optimization, cell engineering, and electrode modifications, may dramatically suppress this spontaneous current leakage.[28]

A comparison of the performance of the presented system with other reported ALBs is given in Table S1. Our system provided a performance higher than or comparable with other ALB systems in terms of capacity and efficiency values and superior long-term stability.

This work presents a new cost-effective aqueous electrolyte solution comprising 14 M LiCl + 4 M CsCl. This solution provides stable behavior of a TiO_2 anode without any significant parasitic contributions. Because costly LiTFSI-based electrolytes are typically considered the preferable solution for ALBs, our findings propose an alternative practical option that shows superior electrochemical performance of a TiO_2 anode and a full TiO_2|LMO cell as well. Although a commonly accepted reason for the improved stability in highly concentrated aqueous electrolytes relates to formation of anodic passivation films,[29] which increases the water splitting overpotential, the lack of organic SEI-forming species in the Li-Cs electrolyte demand an alternative explanation for the superior system stability. Based on the presented results it is possible to ascribe this behavior to three major factors. First, the high Li concentration in the LiCl electrolyte (more than 2.5 times over the commonly used LiTFSI) shifts the Li^+ insertion potential to more positive values, away from the HER. Second, addition of Cl^- ions to the electrolyte results in an increase in the number of Cl···H bonds,

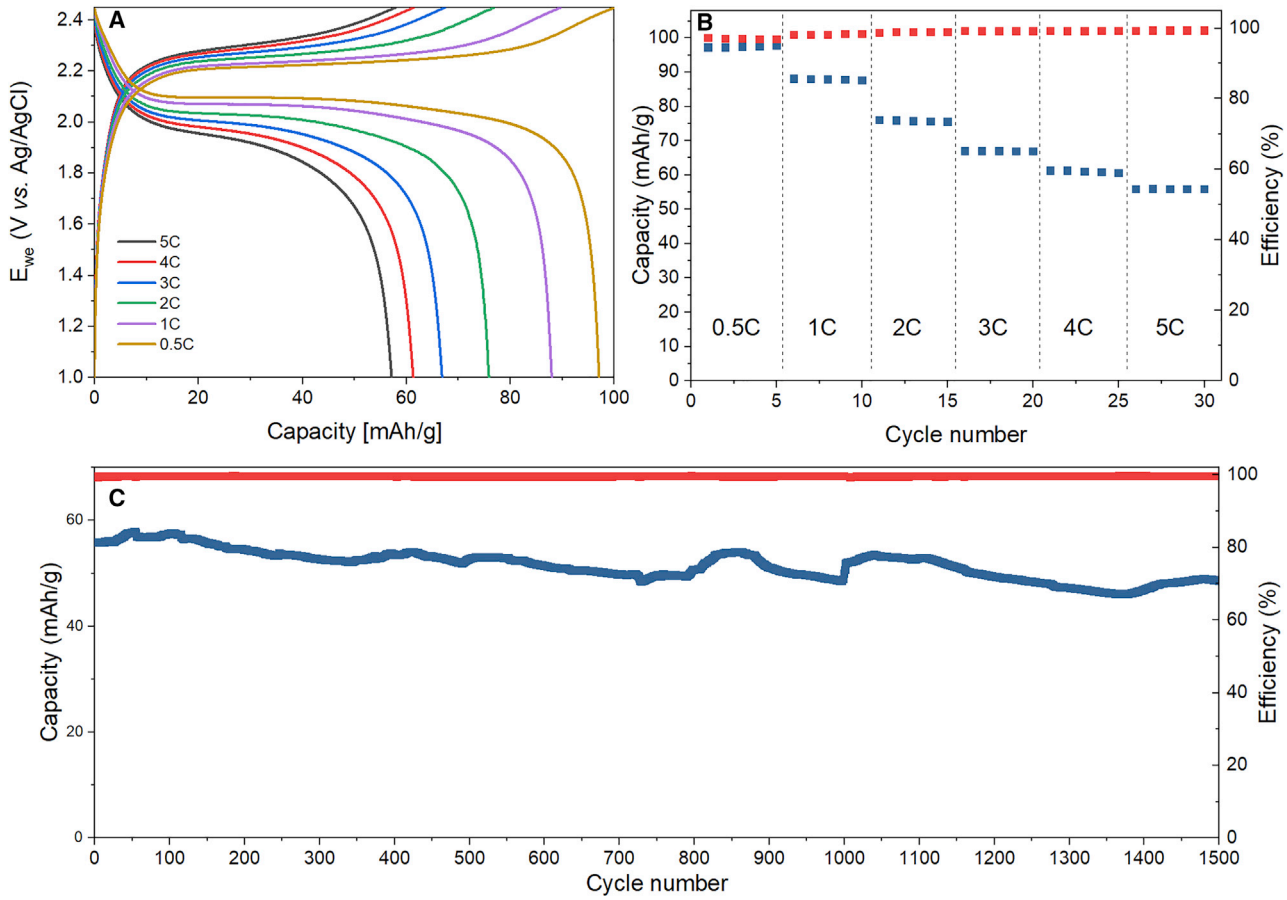

Figure 8. The electrochemical performance of the TiO_2|LMO cell in the mixed Li-Cs electrolyte solution

(A) GCD profiles of TiO_2|LMO at different C rates.

(B) Capacity and efficiency values recorded for each charging rate.

(C) Full cell cycling performance recorded over 1,500 cycles.

which further reduces the hydrogen activity. Third, the presence of Cs^+ ions in the solution acts as a protective double layer that blocks interactions between the water and the anode surface. In this context, the use of chaotropic ions/molecules for HER suppression may be an interesting direction for further development of advanced aqueous batteries.

A major drawback of our developed electrolyte solution is the high Cl^- concentration, which results in a limited positive potential. Nevertheless, several cathodes can be stably applied as positive electrodes, and a high-voltage TiO_2|LMO cell showing high capacity and impressive cyclability was demonstrated successfully. The work presented here provides a highly effective strategy that combines development of new electrolyte solutions and optimization of electrode/electrolyte interfaces. These approaches can be utilized for further development of cost-effective and sustainable aqueous batteries.

EXPERIMENTAL PROCEDURES

Resource availability

Lead contact

Further information and requests for resources should be directed to and will be fulfilled by the lead contact, Netanel Shpigel (nshpigel@gmail.com).

Materials availability

Nano-sized TiO_2 particles, LiCl and CsCl salts, and LFP and V_2O_5 powders were purchased from Sigma-Aldrich.

Data and code availability

All data generated and analyzed during this study are included in this article and the supplemental information. The paper does not report any original code.

Electrode preparation

Micro-sized TiO_2 powder was synthesized according to the following procedure. The spherical micro-sized TiO_2 particles were synthesized through combination of the modified sol-gel and solvothermal method.[1] In a typical synthesis, 1 mL $TiCl_4$ (Sigma-Aldrich) was added dropwise to a mixed solution containing 35 mL isopropanol and 12 mL acetone (v/v) in a beaker. The mixed solution was stirred at room temperature for an additional 30 min in the beaker. This experiment was carried out in an argon-filled glove box. After vigorous stirring, the obtained light-yellow transparent reaction mixture (sol) was further transferred to a 100-mL Teflon-lined still autoclave and heated at 200°C for 12 h. The obtained white precipitate was collected and washed several times with deionized water followed by ethanol to remove impurities and dried in a vacuum at 80°C for 24 h. Finally, the white powder was calcined in air at 400°C for 4 h (2°/min ramping), and crystalline spherical TiO_2 particles were obtained.

The electrodes were prepared by mixing the active-material particles with carbon super-p and polyvinylidene fluoride (PVDF) (mass ratio of 80:10:10) in an NMP solution. The homogenized slurry was coated on grafoil current collectors (0.02-mm thickness) and dried overnight at 80°C.

LMO particles (MTI, USA) were mixed with carbon super-p and PVDF in an NMP solution to obtain a mass ratio of 80:10:10. The homogenized slurry was coated on grafoil film and dried overnight at 80°C.

Electrochemical measurements

All electrochemical tests were carried out using a SP-300 potentiostat/galvanostat (Bio-Logic, France). Three electrode cell measurements were conducted in homemade T cells using excessive carbon cloth and Ag/AgCl as a counter and reference electrode, respectively.

Full cell assembly was done in T cell configuration and repeated in pouch cell configuration. Because of the limited positive working potential of the cathode, the electrodes were balanced at a mass ratio of 1:2.5 TiO_2:LMO.

Physical and morphological characterization

Raman measurements were performed on HOPG electrodes using an integrated laser and a three-VHG-filter system (ONDAX, XLF-MICRO, 532 nm) with 50 mW of optical power at an excitation wavelength of λ_{ex} = 532 nm. The laser output was routed into a lab-built microscope, and the Raman signal was fiber-coupled into an imaging spectrometer (Princeton Instruments, SP-2500i) with an electron microscope charge-coupled device (CCD) camera (Princeton Instruments, Pro-EM 1600).[2] The acquisition duration was around 100 s per measurement, and a grating with a groove density of 600 g/mm was used. At least 10 different spots were measured from each electrode. The baselines of the spectra were shifted for presentation purposes.

HR-scanning electron microscopy (SEM) imaging was performed using a Magellan XHR 400L FE scanning electron microscope (FEI) equipped with an EDS detector (Oxford Instruments).

MD simulations were performed using the CHARMM[1,2] and NAMD[3,4] programs. Initial system construction, heating, and equilibration were performed using CHARMM, whereas NAMD was used for production runs. The initial force field parameters were based on standard values for Li^+ ions,[5] Cl^- ions, and Cs^+ ions.[6,7] To be able to treat the highly concentrated water-in-salt solutions, the force field parameters were fine-tuned by comparison with PBE0 with the aug-cc-pVTZ basis set for all atoms (except def2-TZVPPD for Cs^+)[8–13] and use of the NBFIX option in CHARMM.[14]

Reference energies for ionic interactions

The initial vdW parameters for Cs^+, Li^+, and Cl^- and for the TIP3P[5,15] water model were taken from the CHARMM toppar_ion_water parameter file.[6] As detailed below, some of the ion vdW parameters were modified in this work using the NBFIX strategy.[14] Using this approach, we recalibrated the interactions of ions with their coordinating chemical groups without affecting the interaction of the ions with other chemical groups. The changes were made specifically for the systems we examined in this study, and further work needs to be done to examine transferability to other systems.

The MD simulations of "water in salt" systems were performed with a classical force field (FF). These systems are highly charged; therefore, we ensured that the lack of polarizability terms in the FF did not affect the accuracy of the many-body binding interactions of ion-water clusters. The binding interactions of ionic clusters were tested against quantum chemistry data calculated at PBE08 with Grimme's D3 semi-empirical dispersion corrections[10] with basis sets of aug-cc-pVTZ for all atoms besides Cs^+, which used the def2-TZVPPD basis set. Previous works[12,13,16] benchmarked ionic interactions for clusters calculated at PBE0-TS11against the "gold standard" of LNO-CCSD(T). These studies showed that this DFT method is a valid reference for ionic interactions and that the energy difference relative to LNO-CCSD(T) is less than 1 kcal/mol. Comparing the binding energies of Li^+ water clusters with 1–4 water molecules, calculated at PBE0-D3 (this work) with the corresponding PBE0-TS energies, presents good consistency between the methods, where the energetic difference is below 1 kcal/mol.

Comparing the binding energies for the QM reference with the classical model results

In this work, we chose the CHARMM36 FF for calculating the binding energies for Cs^+-water clusters, Cl^--water clusters, and Li^+-water clusters.

The cluster formation is given by the equation

$$Ion + n(water) \rightarrow Ion(water)_n$$

where n is the number of water molecules in the cluster. n values were changed from one to six for the Cs^+ and Cl^- clusters, whereas the Li^+ clusters included one to four water molecules. The binding energy is defined as

$$E_{Binding} = E_{Ion(water)n} - E_{Ion} - n * E_{water}$$

The clusters with Cs^+ ions and the clusters with Cl^- ions gave good accuracy compared with the quantum chemistry reference, with root mean square (RMS) errors of 1.1 kcal/mol and 2.5 kcal/mol, respectively. On the other hand, the clusters with Li^+ with water yielded a too high error of 15.1 kcal/mol. The pairwise vdW

interaction between Li^+ and water oxygen was recalibrated using the NBFIX strategy and reduced the RMS error to 5.7 kcal/mol. We noticed that the error grows with cluster size, which may be related to many-body interactions.

Because electrostatics are long-range interactions, the binding energies of ion-ion interaction as a function of the distance between the ions were compared with the quantum chemistry reference. The repulsive interactions of Cs^+-Cs^+, Li^+-Li^+, and Cl^--Cl^- were checked at distances ranging between 3–15 Å and presented good accuracy compared with the quantum chemistry baseline. The attractive interactions of Cs^+ with Cl^- and of Li^+ with Cl^- were also computed at distances ranging from 3–15 Å. Here we found that the parameters of the model underbind for the Li^+-Cl^- interaction and overbind for the Cs^+Cl^- interaction compared with the PBE0-D3 values. Modifying the vdW pairwise interactions between Cs^+ with Cl^- and between Li^+ and Cl^- using NBFIX reduced the error at the minima from −8.9 kcal/mol to 0.2 kcal/mol for Cs^+-Cl^- and from 25.5 kcal/mol to 3.5 kcal/mol for Li^+-Cl^-.

MD simulation protocol

MD simulations of three replicas of 14 M LiCl and three replicas of 14 M LiCl + 4 M CsCl were performed in the NPT ensemble using NAMD package 17 and the CHARMM36 FF.[14,18,20] The parameters for the ions and water were taken from the toppar_ion_water parameter file, with some modifications for the pairwise vdW interactions, as discussed above.

The energy of each model was minimized using ABNR, and the ions were explicitly solvated in a TIP3P water box with a size of 30 × 30 × 30 $Å^3$. The three duplications of the two system configurations were done for statistical purposes. Specifically, the three replicas for each system were obtained from extensive Monte Carlo (MC) simulations that were initiated from random "water in salt" configurations. All setup, MC, and MD stages of heating and equilibration used the CHARMM program, followed by 200 ns of MD simulations using the NAMD package. All models ran under the same conditions: a constant pressure of 1 atm and a constant temperature of 298 K, which was controlled by a Langevin thermostat.[22] The MD simulations ran under periodic boundary conditions with Ewald summation for the electrostatic interactions[24] with a cutoff of 14.0 Å. The short-range van der Waals interactions were computed within a cutoff of 12.0 Å and switched off smoothly via a switching function in the range of 10.0–12.0 Å.

SUPPLEMENTAL INFORMATION

Supplemental information can be found online at https://doi.org/10.1016/j.xcrp.2021.100688.

ACKNOWLEDGMENTS

N.S. acknowledges the Israel Academy of Sciences and Humanities for financial support. The research presented in this paper was partially funded by the Israeli Smart Transportation Research Center (ISTRC).

AUTHOR CONTRIBUTIONS

Conceptualization, N.S. and M.T.; investigation, N.S., M.T., G.B., A.S., V.B., H.A., B.G., A.N., and T.R.P.; calculations, V.W.-F. and D.T.M.; writing – review & editing, D.T.M., M.N., and M.D.L.; supervision, N.S., D.T.M., and D.A.

DECLARATION OF INTERESTS

The authors declare no competing interests.

Received: April 22, 2021
Revised: November 5, 2021
Accepted: November 18, 2021
Published: December 10, 2021

REFERENCES

1. Wang, Y., Yi, J., and Xia, Y. (2012). Recent progress in aqueous lithium-ion batteries. Adv. Energy Mater. *2*, 830–840.

2. Suo, L., Borodin, O., Gao, T., Olguin, M., Ho, J., Fan, X., Luo, C., Wang, C., and Xu, K. (2015). "Water-in-salt" electrolyte enables high-voltage aqueous lithium-ion chemistries. Science *350*, 938–943.

3. Suo, L., Oh, D., Lin, Y., Zhuo, Z., Borodin, O., Gao, T., Wang, F., Kushima, A., Wang, Z., Kim, H.C., et al. (2017). How Solid-Electrolyte Interphase Forms in Aqueous Electrolytes. J. Am. Chem. Soc. *139*, 18670–18680.

4. Eftekhari, A. (2018). High-Energy Aqueous Lithium Batteries. Adv. Energy Mater. *8*, 1801156.

5. Zhang, H., Liu, X., Li, H., Hasa, I., and Passerini, S. (2021). Challenges and Strategies for High-Energy Aqueous Electrolyte Rechargeable Batteries. Angew. Chem. Int. Ed. *60*, 598–616.

6. Chao, D., Zhou, W., Xie, F., Ye, C., Li, H., Jaroniec, M., and Qiao, S.Z. (2020). Roadmap for advanced aqueous batteries: From design of materials to applications. Sci. Adv. *6*, eaba4098.

7. Wrogemann, J.M., Künne, S., Heckmann, A., Rodríguez-Pérez, I.A., Siozios, V., Yan, B., Li, J., Winter, M., Beltrop, K., and Placke, T. (2020). Development of Safe and Sustainable Dual-Ion Batteries Through Hybrid Aqueous/Nonaqueous Electrolytes. Adv. Energy Mater. *10*, 1902709.

8. Droguet, L., Grimaud, A., Fontaine, O., and Tarascon, J.M. (2020). Water-in-Salt Electrolyte (WiSE) for Aqueous Batteries: A Long Way to Practicality. Adv. Energy Mater. *10*, 2002440.

9. Liu, J., Yi, L., Liu, L., and Peng, P. (2015). LiV3O8 nanowires with excellent stability for aqueous rechargeable lithium batteries. Mater. Chem. Phys. *161*, 211–218.

10. Kühnel, R.S., Reber, D., Remhof, A., Figi, R., Bleiner, D., and Battaglia, C. (2016). "Water-in-salt" electrolytes enable the use of cost-effective aluminum current collectors for aqueous high-voltage batteries. Chem. Commun. (Camb.) *52*, 10435–10438.

11. Kim, Y.S., Kriegel, S., Harris, K.D., Costentin, C., Limoges, B., and Balland, V. (2017). Evidencing Fast, Massive, and Reversible H+ Insertion in Nanostructured TiO2 Electrodes at Neutral pH. Where Do Protons Come From? J. Phys. Chem. C. *121*, 10325–10335.

12. Choe, C., Lademann, J., and Darvin, M.E. (2016). Depth profiles of hydrogen bound water molecule types and their relation to lipid and protein interaction in the human stratum corneum in vivo. Analyst (Lond.) *141*, 6329–6337.

13. Unal, M., and Akkus, O. (2018). Shortwave-infrared Raman spectroscopic classification of water fractions in articular cartilage ex vivo. J. Biomed. Opt. *23*, 1–11.

14. Hu, Q., and Zhao, H. (2019). Understanding the effects of chlorine ion on water structure from a Raman spectroscopic investigation up to 573 K. J. Mol. Struct. *1182*, 191–196.

15. Harsányi, I., and Pusztai, L. (2012). Hydration structure in concentrated aqueous lithium chloride solutions: a reverse Monte Carlo based combination of molecular dynamics simulations and diffraction data. J. Chem. Phys. *137*, 204503.

16. Baranauskaite, V., Pestova, O., Vovk, M., Matveev, V., and Lähderanta, E. (2019). Local dynamics in LiCl-CsCl-D_2O water-in-salt solutions according to NMR relaxation. Phys. Chem. Chem. Phys. *21*, 22895–22901.

17. Huang, B., Rao, R.R., You, S., Myint, K.H., Song, Y., Wang, Y., Ding, W., Giordano, L., Zhang, Y., Wang, T., et al. (2021). Cation- and pH-Dependent Hydrogen Evolution and Oxidation Reaction Kinetics. JACS Au. *11*, jacsau.1c00281.

18. Dubouis, N., Serva, A., Salager, E., Deschamps, M., Salanne, M., and Grimaud, A. (2018). The fate of water at the electrochemical interfaces: electrochemical behavior of free water vs. coordinating water. J. Phys. Chem. Lett. *9*, 6683–6688.

19. Lim, J., Park, K., Lee, H., Kim, J., Kwak, K., and Cho, M. (2018). Nanometric Water Channels in Water-in-Salt Lithium Ion Battery Electrolyte. J. Am. Chem. Soc. *140*, 15661–15667.

20. Singh, M.B., Dalvi, V.H., and Gaikar, V.G. (2015). Investigations of clustering of ions and diffusivity in concentrated aqueous solutions of lithium chloride by molecular dynamic simulations. RSC Adv. 15328–15337.

21. Hou, X., Ju, X., Zhao, W., Wang, J., He, X., Du, L., Yan, B., Li, J., Paillard, E., Sun, J., et al. (2021). TiO2@LiTi2(PO4)3 enabling fast and stable lithium storage for high voltage aqueous lithium-ion batteries. J. Power Sources *484*, 229255.

22. Subramanya, U., Chua, C., He Leong, V.G., Robinson, R., Cruz Cabiltes, G.A., Singh, P., Yip, B., Bokare, A., Erogbogbo, F., and Oh, D. (2019). Carbon-based artificial SEI layers for aqueous lithium-ion battery anodes. RSC Adv. *10*, 674–681.

23. Lukatskaya, M.R., Feldblyum, J.I., Mackanic, D.G., Lissel, F., Michels, D.L., Cui, Y., and Bao, Z. (2018). Concentrated mixed cation acetate "water-in-salt" solutions as green and low-cost high voltage electrolytes for aqueous batteries. Energy Environ. Sci. *11*, 2876–2883.

24. Li, M., Zhang, Y., Hassan, F., Ahn, W., Wang, X., Liu, W.W., Jiang, G., and Chen, Z. (2017). Compact high volumetric and areal capacity lithium sulfur batteries through rock salt induced nano-architectured sulfur hosts. J. Mater. Chem. A Mater. Energy Sustain. *5*, 21435–21441.

25. Xiao, Y., Hwang, J.Y., and Sun, Y.K. (2017). Micro-Intertexture Carbon-Free Iron Sulfides as Advanced High Tap Density Anodes for Rechargeable Batteries. ACS Appl. Mater. Interfaces *9*, 39416–39424.

26. Angulo, A., van der Linde, P., Gardeniers, H., Modestino, M., and Fernández Rivas, D. (2020). Influence of Bubbles on the Energy Conversion Efficiency of Electrochemical Reactors. Joule *4*, 555–579.

27. Jeon, D.H. (2019). Wettability in electrodes and its impact on the performance of lithium-ion batteries. Energy Storage Mater. *18*, 139–147.

28. Liu, K., Yu, C., Guo, W., Ni, L., Yu, J., Xie, Y., Wang, Z., Ren, Y., and Qiu, J. (2021). Recent research advances of self-discharge in supercapacitors: Mechanisms and suppressing strategies. J. Energy Chem. *58*, 94–109.

29. Dubouis, N., Lemaire, P., Mirvaux, B., Salager, E., Deschamps, M., and Grimaud, A. (2018). The role of the hydrogen evolution reaction in the solid-electrolyte interphase formation mechanism for ": Water-in-Salt " electrolytes. Energy Environ. Sci. *11*, 3491–3499.